JACS
JOURNAL OF THE AMERICAN CHEMICAL SOCIETY
pubs.acs.org/JACS
Communication

Pushing Limits of Ultra-wideline Solid-State NMR Spectroscopy: NMR Signatures of ^{209}Bi and ^{127}I in Metal−Organic Frameworks at Ultra-high Magnetic Fields

Wanli Zhang, Yijue Xu, Amrit Venkatesh, Ivan Hung, Shuting Li, Zhehong Gan, and Yining Huang*

Cite This: J. Am. Chem. Soc. 2025, 147, 10823−10828
Read Online

ABSTRACT: Bismuth- and iodine-containing metal−organic frameworks (MOFs) are crucial in catalysis, gas adsorption, and luminescence, with local environments of Bi and I ions shaping their performance. Using ^{209}Bi and ^{127}I solid-state NMR (SSNMR) for characterization is extremely challenging due to the exceedingly large quadrupolar interactions in MOFs. Here, we present ultra-wideline (UW) SSNMR spectra of eight MOFs acquired at ultra-high magnetic fields up to 36 T, with breadths of 8−50 MHz, revealing very large quadrupolar couplings. These spectra uncover key structural details, including dehydration, guest adsorption, phase transitions, and disorder. This study establishes ^{209}Bi and ^{127}I UW SSNMR as powerful tools for probing Bi and I ions in weight-dilute systems, offering broad applications in catalysis, solar cells, biochemistry, and beyond.

Metal−organic frameworks (MOFs) are crystalline porous materials with diverse applications.[1] Bismuth-based MOFs, known for their biocompatibility, low-toxicity, and strong iodine affinity,[2,3] excel in catalysis,[4,5] biomedical imaging,[6] and radionuclide capture.[7] Iodine-containing MOFs, with electron-rich structures and semiconducting properties,[8] are promising for photocatalysis,[9] photoluminescence,[10] and iodine capture.[11] Advancing MOF design requires atomic-level insights into bismuth and iodide behavior. Single-crystal XRD relies on large, high-quality crystals, which are not always attainable. Solid-state NMR (SSNMR) has proven to be a powerful complementary technique for MOF characterization.[12−15]

While ^{209}Bi and ^{127}I SSNMR faces significant experimental challenges,[16−23] the NMR applications of these nuclei in MOFs remain underexplored. ^{209}Bi (I = 9/2) and ^{127}I (I = 5/2) are the only NMR-active isotopes of bismuth and iodine, respectively. Although both isotopes exhibit high receptivity (large gyromagnetic ratios: $\gamma(^{209}\mathrm{Bi}) = 4.375 \times 10^7$ rad·T^{-1}·s^{-1}, $\gamma(^{127}\mathrm{I}) = 5.390 \times 10^7$ rad·T^{-1}·s^{-1}) with 100% natural abundance, their quadrupole moments are very large ($Q(^{209}\mathrm{Bi}) = -51.6$ fm^2, $Q(^{127}\mathrm{I}) = -71.0$ fm^2).[24] In MOFs, Bi and I are often in low-spherical symmetry environments and experience exceedingly large quadrupolar interactions, causing extremely broad SSNMR spectra spanning tens of MHz.[25] Nuclei like ^{209}Bi with high spin and large quadrupole moments also have intense satellite transitions (STs) closely "packed" around the central transition (CT), exhibiting significant third-order effects and complicating the acquisition and interpretation of ultra-wideline (UW) SSNMR spectra.[17] Reducing quadrupolar broadening in half-integer nuclei can be achieved by performing SSNMR at ultra-high magnetic fields, where second-order quadrupolar interaction (QI) is inversely proportional to the applied field.[26] Recent advances in 36 T magnets[27] enable the acquisition of UW SSNMR spectra for challenging nuclei like ^{209}Bi and ^{127}I.

Many bismuth- and iodine-containing materials have been studied using ^{209}Bi and ^{127}I nuclear quadrupole resonance (NQR).[18,28−37] NQR offers advantages such as narrow lines (better resolution), direct reflection of QI parameters, and lower cost (greater accessibility). When quadrupolar frequencies exceed the Larmor frequency, NQR or Zeeman-perturbated NQR becomes particularly effective to probe the QI.[38,39] However, challenges include time-intensive signal searches in unknown samples[38,39] and short spin−spin relaxation (T_2) times for samples with large C_Q values,[40] complicating detection. An excellent review[39] provides detailed comparisons of solid-state NMR and NQR. ^{209}Bi and ^{127}I NQR experiments on the MOFs were conducted in the predicted frequency ranges. However, no signals were observed (See SI, page S4 for details).

Here, we demonstrate that ^{209}Bi and ^{127}I UW SSNMR spectra of MOFs with breadths spanning tens of MHz can be acquired efficiently at 36 T, revealing sensitivity to coordination environment changes due to activation, phase transitions, guest adsorption, and disorder. Normally acquiring powder patterns broader than 1 MHz on a superconducting magnet requires VOCS (variable offset cumulative spectrum)[41] technique. The UW SSNMR spectra are reconstructed from multiple subspectra obtained by stepping the transmitter frequency. However, in the 36 T series-connected hybrid magnet used in this study, the probe cannot be accessed for

Received: December 9, 2024
Revised: March 1, 2025
Accepted: March 4, 2025
Published: March 19, 2025

https://doi.org/10.1021/jacs.4c17499
J. Am. Chem. Soc. 2025, 147, 10823−10828

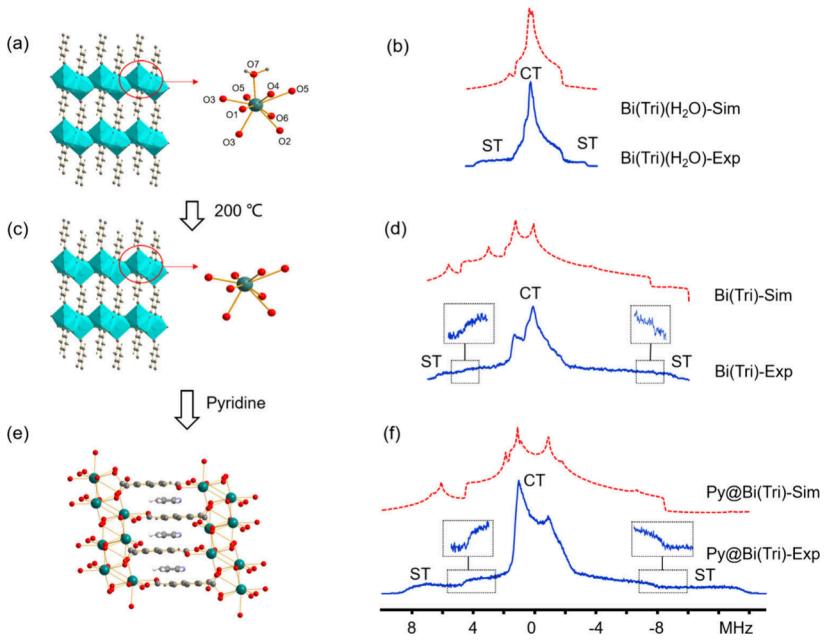

Figure 1. Schematic illustration of Bi local geometry in (a) Bi(Tri)(H_2O),[45] (c) Bi(Tri) and (e) Py@Bi(Tri), as well as experimental (blue, Exp) and simulated (red, Sim) ^{209}Bi UW SSNMR spectra of (b) Bi(Tri)(H_2O), (d) Bi(Tri) and (f) Py@Bi(Tri). Both CT and STs are considered in the simulation (see Figures S5–S7 for specific signal assignments of different transitions). The magnified view of "edges" is shown in the insets.

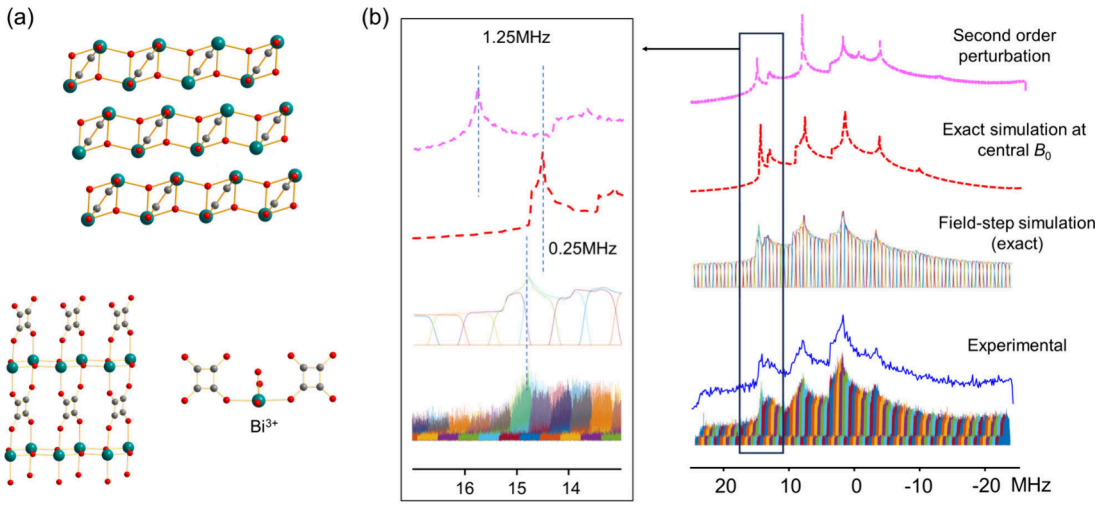

Figure 2. (a) Layered structure of MOF IEF-3 and the Bi coordination geometry. (b) Experimental and simulated ^{209}Bi UW SSNMR spectra of IEF-3 using three simulation protocols. The magnified view of the "horn" at *ca.* 15 MHz is shown in the inset.

tuning above 18 T. Instead, the field is varied while transmitter frequency remains fixed.[42−44] For ^{209}Bi, spectral width can exceed 50 MHz, requiring field-stepping over 7.2 T. The field-stepped acquisition strategy, as outlined in refs43, 44, is illustrated in Scheme S1.

This work extends UW SSNMR limits, achieving unprecedented spectral breadths and showcasing its power at ultra-high fields to uncover local structures in Bi- and I-containing MOFs and beyond.

^{209}Bi UW SSNMR of MOFs. Bismuth-carboxylate MOFs offer versatile catalytic and luminescent properties,[2] with photoluminescence tunable via linkers' carboxylate groups.[45] Bi(Tri)(H_2O) (Tri = trimellitate) has a 3D structure (Figure 1(a)), featuring edge-sharing BiO_9 chains linked by trimellitate, where Bi^{3+} coordinates to eight carboxylate oxygens and one water oxygen in an irregular polyhedron (Figure S3).[45] The ^{209}Bi UW SSNMR spectrum (Figure 1(b)) is reconstructed from 22 subspectra by stepping the magnetic field from 33.24 to 34.15 T (Figure S4). The CT in the spectrum exhibits a well-defined QI-dominated powder pattern that can be simulated with one Bi site (Table S1; Figure S5(b) with full ST simulation), consistent with crystal structure.[45] The quadrupolar coupling constant, C_Q(^{209}Bi) is 230(1) MHz obtained from the spectral simulation.

Dehydration of Bi(Tri)(H_2O) removes coordinated water, leaving Bi(Tri) with a similar ordered structure, as shown by comparable PXRD patterns (Figure S1). However, their ^{209}Bi spectra differ remarkably (Figure 1(d)): dehydration doubles C_Q from 230(1) to 470(1) MHz, reflecting reduced spherical symmetry and a shift from nine- to eight-coordinate Bi centers. Plane-wave DFT calculations predict C_Q values of 298 MHz for Bi(Tri)(H_2O) and 422 MHz for Bi(Tri) (Table S4). The

https://doi.org/10.1021/jacs.4c17499
J. Am. Chem. Soc. 2025, 147, 10823−10828

unsaturated Bi^{3+} in dehydrated Bi(Tri) makes it a potential adsorbent. Exposing Bi(Tri) to pyridine forms Py@Bi(Tri) with an unknown structure. But its PXRD pattern (Figure S1) is similar to Bi(Tri), indicating that both have comparable long-range order. Compared to Bi(Tri), Py@Bi(Tri) exhibits a ^{209}Bi isotropic shift at a higher field and a similar C_Q (Table S1, Figure 1(f)). There are two possible positions for pyridine in Bi(Tri): interacting with Bi^{3+} through its nitrogen or forming $\pi-\pi$ interactions with the linkers. Our plane-wave DFT calculations (Figure S8) model both scenarios. Pyridine binding to Bi^{3+} via its N atom predicts a much larger C_Q than Bi(Tri), contradicting experimental data. Instead, calculations show minimal C_Q change when pyridine engages in $\pi-\pi$ interactions with linkers, suggesting it interacts with linkers, as observed in other pyridine-loaded MOFs like SION-82.[46] This aligns with pyridine's larger size, which hinders coordination to Bi via the N atom in confined spaces.

Many bismuth MOFs, like IEF-3 ($Bi_2O_2(C_4O_4)$),[47] are studied for photocatalysis due to their semiconducting properties. Synthesized hydrothermally from $Bi(NO_3)_3$ and squaric acid, IEF-3 features a layered structure (Figure 2(a)), where Bi^{3+} forms a distorted square pyramid by coordinating with three bridging O^{2-} ions and two oxygens from two squarate linkers.[47] The ^{209}Bi UW SSNMR spectrum was reconstructed from 100 subspectra obtained by field-stepping over 7.2 T and exhibits a complex line shape spanning over 45 MHz (Figure 2(b)), despite having a single Bi site. It displays five distinctive features from both CT and STs. Due to the large C_Q, the high-field CT edge is not observed, but the three horns from STs (between 5−15 MHz) enable accurate spectrum simulation (Table S1, Figure S9 for assignments).

To accurately simulate the ^{209}Bi UW SSNMR spectrum of IEF-3, two factors need to be considered. (1) The very large quadrupolar interactions (ν_Q/ν_0 = 16%, where the quadrupolar frequency is expressed as $\nu_Q = \frac{3C_Q}{2I(2I-1)}$) lead to the breakdown of the second-order perturbation theory, even at ultra-high magnetic fields.[48] Figure 2(b) shows the low field "horn" of simulated spectra with the second-order perturbation theory and "exact" method using the direct diagonalization of Hamiltonian, yielding a difference of *ca.* 1.25 MHz. (2) Due to the large number of field steps needed to reconstruct the complete spectrum, it is necessary to perform field-stepped exact simulation of 100 subspectra from 28.6 to 35.8 T to calibrate the magnetic shielding and quadrupolar interactions at different fields as both are field-dependent.[43] Compared to the exact simulation at the central magnetic field, the "horn" at low field region in the field-stepped exact simulation differs by approximately 0.25 MHz (Figure 2b). The C_Q of 860(2) MHz is among the very large C_Q values ever reported in NMR experiments,[49,50] and is substantially larger than those observed in Bi sites of non-MOF materials.[16,17] This is attributed to the very low spherical symmetry of Bi^{3+} in its square-pyramidal geometry (BiO_5) in IEF-3, where the coordinated five oxygens are distributed within the same hemisphere around Bi^{3+}. The plane-wave DFT calculation on the fully optimized structure yields a calculated $C_{Q,cal}$ = 727 MHz.

According to hard−soft acid−base theory, Bi^{3+}, a borderline acid, binds to both oxygen and nitrogen donors. Reaction using pyridine-3,5-dicarboxylic acid (PDC) with carboxylate and pyridine groups forms the MOF ARL-3 ($Bi_2O_2[NC_5H_3(CO_2)_2]$) (Figure S10(a)). ARL-3 features 1D cationic $[Bi_2O_2]^{2+}$ chains linked by PDC into a 3D MOF, with two unique Bi sites: BiO_7 and BiO_5N (Figure S10(a)).[51] The ^{209}Bi UW SSNMR spectrum exhibits several features, which cannot be well simulated with a single Bi site. Instead, it is better simulated using 2 sites (Figure S10(b), Table S1). To assign the two resonances, plane-wave DFT and cluster DFT calculations were performed for ^{209}Bi EFG tensors (Table S4 and S5). The calculated orders, $C_Q(BiO_7) > C_Q(BiO_5N)$ and $\eta_Q(BiO_7) > \eta_Q(BiO_5N)$, are used to assign the signals to their respective Bi sites with site 1 assigned to BiO_7 and site 2 to BiO_5N.

^{127}I UW SSNMR of MOFs. Iodides in MOFs can enhance catalysis with suitable metals, as seen in Cu(I)-X-bpy MOFs (X = Cl, Br, I; bpy = 4,4′-bipyridine), showing potential for photocatalytic hydrogen production.[9] In [CuI(bpy)], iodide

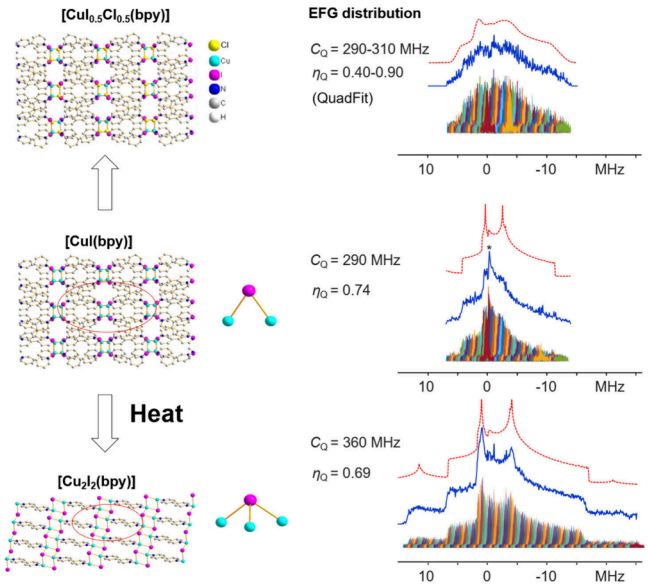

Figure 3. Schematic illustrations of MOFs [CuI(bpy)], [Cu_2I_2(bpy)] and [$CuI_{0.5}Cl_{0.5}$(bpy)]; experimental (blue) and simulated (red) ^{127}I UW SSNMR spectra of the three MOFs. The sharp signal (*) near 0 ppm comes from CuI impurity.

bridges two Cu(I) centers in a μ_2 configuration (Figure 3). Its ^{127}I UW SSNMR spectrum exhibits QI-dominated powder pattern with a breadth of *ca.* 20 MHz reconstructed from 73 subspectra stepping from 32.1 to 34.3 T. The coadded spectrum can be simulated using one iodide site (Table S1), consistent with the crystal structure.[52] The 3D [CuI(bpy)] can be transformed to 2D [Cu_2I_2(bpy)] by heating,[52,53] where the iodide converts from the μ_2 to μ_3 configuration (Figure 3). The ^{127}I UW SSNMR spectra of [CuI(bpy)] and [Cu_2I_2(bpy)] look distinctly different. The $C_Q(^{127}I)$ of 290(2) MHz in [CuI(bpy)] increases to 360(2) MHz in [Cu_2I_2(bpy)] (Table S1), reflecting the decreased spherical symmetry due to the configuration change from μ_2- to μ_3-I. The η_Q parameter is also sensitive to the phase change, falling from 0.74 to 0.69 after phase change, reflecting increased axial symmetry about the iodide.

Introducing secondary halide ions into [CuI(bpy)] forms mixed-anion MOFs [CuI_xCl_{1-x}(bpy)] with tunable photocatalytic hydrogen production.[54] Halide disorder makes characterization by PXRD challenging. For x = 0.5, reacting 4,4′-bipyridine with equimolar CuCl and CuI produces [$CuI_{0.5}Cl_{0.5}$(bpy)]. The simulated and experimental PXRD

https://doi.org/10.1021/jacs.4c17499
J. Am. Chem. Soc. 2025, 147, 10823−10828

patterns of $[CuI_{0.5}Cl_{0.5}(bpy)]$ closely align (Figure S2), confirming its identity and purity. Both $[CuI_{0.5}Cl_{0.5}(bpy)]$ and [CuI(bpy)] crystallize in the same space group (*I*41/*acd*),[54] resulting in similar PXRD patterns, with minor differences in peak positions and line width arising from variations in unit cell parameters and local disorder. The Cl:I ratio was determined by EDX and XPS (Figure S11). The appearance of the ^{127}I UW SSNMR spectrum of $[CuI_{0.5}Cl_{0.5}(bpy)]$ indicates that the iodide has a partially disordered environment. Thus, we employ the Gaussian distribution model to describe the distributions of the EFG tenor parameters.[55] The ^{127}I UW SSNMR spectrum can be well simulated with a C_Q distribution from 290 to 310 MHz, and an η_Q distribution from 0.40 to 0.90 (Table S1). These distributions can be attributed to two factors. First, there are two possible local coordination environments for iodine $\{Cu_2I_2\}$ and $\{Cu_2ICl\}$ with random spatial distributions within the framework (Figure S12 and the footnote). Second, as observed from single crystal structures of mixed-anion [CuX(byp), X= I, Cl],[54] a relatively large isotropic displacement parameter for iodine indicates that the iodide is not located at a single, well-defined position (note that an isotropic displacement parameter (or U_{iso}) in crystallography quantifies the degree of atomic displacement from an average position due to thermal motion and/or disorder[56]) As a result, the Cu−I−Cu bond lengths and angles may vary across different unit cells.

Some MOFs exhibit multiple inequivalent iodide sites. For example, MOF $[Cu_4I_4(DABCO)_2]$ contains three distinct iodides.[57] We acquired ^{127}I UW SSNMR spectra of this MOF over 3 days to differentiate between these sites. The ^{127}I UW SSNMR spectrum spans *ca.* 60 MHz (Figure S13) and could only be simulated using a single site with C_Q = 530(2) MHz and η_Q= 0.28(2). The lack of resolution between these sites is likely due to their similar environments (Table S6),[57] and the limited acquisition of subspectra, constrained by available magnet time.

In summary, we successfully obtained the ^{209}Bi and ^{127}I UW SSNMR spectra of representative MOFs at ultra-high magnetic fields, overcoming the challenges posed by very large quadrupolar interactions. The extremely broad ^{209}Bi and ^{127}I UW SSNMR spectra are highly sensitive to structural changes induced by dehydration, guest−host interaction, phase transition and local disorder. This study demonstrates the feasibility of direct characterization of nuclei with extremely large quadrupole moments in MOF materials. This approach could be extended to other fields beyond MOFs such as solar cells, surface science, catalysis, and biochemistry.

■ ASSOCIATED CONTENT

Supporting Information

The Supporting Information is available free of charge at https://pubs.acs.org/doi/10.1021/jacs.4c17499.

Experimental details, powder XRD patterns, additional NMR data and simulations, and calculation results (PDF)

■ AUTHOR INFORMATION

Corresponding Author

Yining Huang − *Department of Chemistry, The University of Western Ontario, London, Ontario N6A 5B7, Canada;* orcid.org/0000-0001-9265-5896; Email: yhuang@uwo.ca

Authors

Wanli Zhang − *Department of Chemistry, The University of Western Ontario, London, Ontario N6A 5B7, Canada*

Yijue Xu − *National High Magnetic Field Laboratory, Florida State University, Tallahassee, Florida 32310, United States*

Amrit Venkatesh − *National High Magnetic Field Laboratory, Florida State University, Tallahassee, Florida 32310, United States;* orcid.org/0000-0001-5319-9269

Ivan Hung − *National High Magnetic Field Laboratory, Florida State University, Tallahassee, Florida 32310, United States;* orcid.org/0000-0001-8916-739X

Shuting Li − *Department of Chemistry, The University of Western Ontario, London, Ontario N6A 5B7, Canada*

Zhehong Gan − *National High Magnetic Field Laboratory, Florida State University, Tallahassee, Florida 32310, United States;* orcid.org/0000-0002-9855-5113

Complete contact information is available at: https://pubs.acs.org/10.1021/jacs.4c17499

Notes

The authors declare no competing financial interest.

■ ACKNOWLEDGMENTS

Y.H. thanks the Natural Science and Engineering Research Council (NSERC) of Canada for a Discovery Grant. The National High Magnetic Field Laboratory is supported by the National Science Foundation through NSF/DMR-1644779 and NSF/DMR-2128556, and the State of Florida. The SCH magnet and NMR instrumentation was supported by the NSF (DMR-1039938 and DMR-0603042) and NIH (BTRR 1P41 GM122698 and RM1GM148766). This work was made possible by the facilities of the Shared Hierarchical Academic Research Computing Network (SHARCNET: http://www.sharcnet.ca), Compute/Calcul Canada, and the Digital Research Alliance of Canada.

■ REFERENCES

(1) Furukawa, H.; Cordova, K. E.; O'Keeffe, M.; Yaghi, O. M. The Chemistry and Applications of Metal-Organic Frameworks. *Science (80-.).* **2013**, *341* (6149), 1230444.

(2) Wang, Z.; Zeng, Z.; Wang, H.; Zeng, G.; Xu, P.; Xiao, R.; Huang, D.; Chen, S.; He, Y.; Zhou, C.; et al. Bismuth-Based Metal−Organic Frameworks and Their Derivatives: Opportunities and Challenges. *Coord. Chem. Rev.* **2021**, *439*, 213902.

(3) Wang, W.; Zeng, D.; Wang, J.; Zhang, Y.; Zhang, L.; Wang, W. Synthesis and Application of Bismuth-Based Metal-Organic Framework. *Prog. Chem.* **2022**, *34* (11), 2405−2416.

(4) Zhang, X.; Zhang, Y.; Li, Q.; Zhou, X.; Li, Q.; Yi, J.; Liu, Y.; Zhang, J. Highly Efficient and Durable Aqueous Electrocatalytic Reduction of CO_2 to HCOOH with a Novel Bismuth−MOF: Experimental and DFT Studies. *J. Mater. Chem. A* **2020**, *8* (19), 9776−9787.

(5) Nguyen, V. H.; Nguyen, T. D.; Van Nguyen, T. Microwave-Assisted Solvothermal Synthesis and Photocatalytic Activity of Bismuth (III) Based Metal−Organic Framework. *Top. Catal.* **2020**, *63* (11), 1109−1120.

(6) Robison, L.; Zhang, L.; Drout, R. J.; Li, P.; Haney, C. R.; Brikha, A.; Noh, H.; Mehdi, B. L.; Browning, N. D.; Dravid, V. P.; et al. A Bismuth Metal−Organic Framework as a Contrast Agent for X-Ray Computed Tomography. *ACS Appl. Bio Mater.* **2019**, *2* (3), 1197−1203.

(7) Reda, A. T.; Pan, M.; Zhang, D.; Xu, X. Bismuth-Based Materials for Iodine Capture and Storage: A Review. *J. Environ. Chem. Eng.* **2021**, *9* (4), 105279.
(8) Li, X.-X.; Zheng, S.-T. Three-Dimensional Metal-Halide Open Frameworks. *Coord. Chem. Rev.* **2021**, *430*, 213663.
(9) Shi, D.; Zheng, R.; Sun, M.; Cao, X.; Sun, C.; Cui, C.; Liu, C.; Zhao, J.; Du, M. Semiconductive Copper (I)−Organic Frameworks for Efficient Light-Driven Hydrogen Generation Without Additional Photosensitizers and Cocatalysts. *Angew. Chem.* **2017**, *129* (46), 14829−14833.
(10) Li, X.-Y.; Wang, Y.-L.; Xue, Z.; Han, S.-D.; Xue, Z.-Z.; Pan, J. Heterometallic−Organic Framework from $[Cu_2I_2]$ and $[PbO]_n$ Chains: Photoluminescence, Sensing, and Photocatalytic Performance. *Cryst. Growth Des.* **2021**, *21* (9), 5261−5267.
(11) He, J.; Duan, J.; Shi, H.; Huang, J.; Huang, J.; Yu, L.; Zeller, M.; Hunter, A. D.; Xu, Z. Immobilization of Volatile and Corrosive Iodine Monochloride (ICl) and I_2 Reagents in a Stable Metal−Organic Framework. *Inorg. Chem.* **2014**, *53* (13), 6837−6843.
(12) Lucier, B. E. G.; Chen, S.; Huang, Y. Characterization of Metal−Organic Frameworks: Unlocking the Potential of Solid-State NMR. *Acc. Chem. Res.* **2018**, *51* (2), 319−330.
(13) Brunner, E.; Rauche, M. Solid-State NMR Spectroscopy: An Advancing Tool to Analyse the Structure and Properties of Metal-Organic Frameworks. *Chem. Sci.* **2020**, *11* (17), 4297−4304.
(14) Xu, J.; Wang, Q.; Deng, F. Metal Active Sites and Their Catalytic Functions in Zeolites: Insights from Solid-State NMR Spectroscopy. *Acc. Chem. Res.* **2019**, *52* (8), 2179−2189.
(15) Fu, Y.; Guan, H.; Yin, J.; Kong, X. Probing Molecular Motions in Metal-Organic Frameworks with Solid-State NMR. *Coord. Chem. Rev.* **2021**, *427*, 213563.
(16) Hamaed, H.; Laschuk, M. W.; Terskikh, V. V.; Schurko, R. W. Application of Solid-State ^{209}Bi NMR to the Structural Characterization of Bismuth-Containing Materials. *J. Am. Chem. Soc.* **2009**, *131* (23), 8271−8279.
(17) Griffith, K. J.; Ding, F.; Flynn, S. Solid-state Nuclear Magnetic Resonance of Spin-9/2 Nuclei ^{115}In and ^{209}Bi in Functional Inorganic Complex Oxides. *Magn. Reson. Chem.* **2021**, *59* (9−10), 1077−1088.
(18) Widdifield, C. M.; Bryce, D. L. Solid-State ^{127}I NMR and GIPAW DFT Study of Metal Iodides and Their Hydrates: Structure, Symmetry, and Higher-Order Quadrupole-Induced Effects. *J. Phys. Chem. A* **2010**, *114* (40), 10810−10823.
(19) Wu, G.; Dong, S. High-Field ^{127}I NMR of Solid Sheelite Structures: Periodates Revisited. *Solid State Nucl. Magn. Reson.* **2001**, *20* (3−4), 100−107.
(20) Taylor, R. E.; Beckmann, P. A.; Bai, S.; Dybowski, C. ^{127}I and ^{207}Pb Solid-State NMR Spectroscopy and Nuclear Spin Relaxation in PbI_2: A Preliminary Study. *J. Phys. Chem. C* **2014**, *118* (17), 9143−9153.
(21) Laurencin, D.; Ribot, F.; Gervais, C.; Wright, A. J.; Baker, A. R.; Campayo, L.; Hanna, J. V.; Iuga, D.; Smith, M. E.; Nedelec, J.; et al. ^{87}Sr, ^{119}Sn, ^{127}I Single and ^{1}H/^{19}F-Double Resonance Solid-State NMR Experiments: Application to Inorganic Materials and Nanobuilding Blocks. *ChemistrySelect* **2016**, *1* (15), 4509−4519.
(22) Lim, A. R.; Choh, S. H.; Jang, M. S. Domain Structure of Ferroelastic $BiVO_4$ Studid by ^{209}Bi NMR. *Solid State Commun.* **1996**, *97* (8), 699−702.
(23) Karmakar, A.; Bernard, G. M.; Pominov, A.; Tabassum, T.; Chaklashiya, R.; Han, S.; Jain, S. K.; Michaelis, V. K. Triangulating Dopant-Level Mn (II) Insertion in a $Cs_2NaBiCl_6$ Double Perovskite Using Magnetic Resonance Spectroscopy. *J. Am. Chem. Soc.* **2023**, *145* (8), 4485−4499.
(24) Pyykkö, P. Year-2017 Nuclear Quadrupole Moments. *Mol. Phys.* **2018**, *116* (10), 1328−1338.
(25) Schurko, R. W. Ultra-Wideline Solid-State NMR Spectroscopy. *Acc. Chem. Res.* **2013**, *46* (9), 1985−1995.
(26) Ashbrook, S. E. Recent Advances in Solid-State NMR Spectroscopy of Quadrupolar Nuclei. *Phys. Chem. Chem. Phys.* **2009**, *11* (32), 6892−6905.
(27) Gan, Z.; Hung, I.; Wang, X.; Paulino, J.; Wu, G.; Litvak, I. M.; Gor'kov, P. L.; Brey, W. W.; Lendi, P.; Schiano, J. L.; Bird, M. D.; Dixon, I. R.; Toth, J.; Boebinger, G. S.; Cross, T. A. NMR Spectroscopy up to 35.2 T Using a Series-Connected Hybrid Magnet. *J. Magn. Reson.* **2017**, *284*, 125−136.
(28) Kawasaki, Y.; Kishimoto, Y.; Imai, N.; Ohno, T.; Kubo, H.; Yoshii, S.; Kasaya, M. ^{209}Bi-NQR Investigation of the Non-Magnetic Heavy-Fermion Compound CeRhBi. *J. Phys. Soc. Jpn.* **2004**, *73* (3), 694−697.
(29) Widdifield, C. M.; Jurca, T.; Richeson, D. S.; Bryce, D. L. Using $^{69/71}$Ga Solid-State NMR and ^{127}I NQR as Probes to Elucidate the Composition of "GaI". *Polyhedron* **2012**, *35* (1), 96−100.
(30) Kitagawa, S.; Ishida, K.; Ishii, W.; Yajima, T.; Hiroi, Z. Nematic Transition and Highly Two-Dimensional Superconductivity in $BaTi_2Bi_2O$ Revealed by ^{209}Bi-Nuclear Magnetic Resonance/Nuclear Quadrupole Resonance Measurements. *Phys. Rev. B* **2018**, *98* (22), 220507.
(31) Kravchenko, E. A.; Orlov, V. G.; Hai Fam, S.; Kargin, Y. F. ^{209}Bi NQR and Magnetic Properties of Bismuth Oxide-Based Compounds. *Zeitschrift für Naturforsch. A* **1998**, *53* (6−7), 504−513.
(32) Ainbinder, N. E.; Volgina, G. A.; Kravchenko, E. A.; Osipenko, A. N.; Gippius, A. A.; Hai Fam, S.; Bush, A. A. ^{209}Bi NQR Powder Spectra Influenced by Local and Applied Magnetic Fields. *Zeitschrift für Naturforsch. A* **1994**, *49* (1−2), 425−432.
(33) Zemnukhova, L. A.; Kuznetsov, S. I.; Davidovich, R. L. ^{209}Bi NQR Study of Bismuth (III) Complexes. *Russ. Chem. Bull.* **1998**, *47*, 2169−2172.
(34) Bryce, D. L.; Sward, G. D. Solid-state NMR Spectroscopy of the Quadrupolar Halogens: Chlorine-35/37, Bromine-79/81, and Iodine-127. *Magn. Reson. Chem.* **2006**, *44* (4), 409−450.
(35) Senocrate, A.; Moudrakovski, I.; Maier, J. Short-Range Ion Dynamics in Methylammonium Lead Iodide by Multinuclear Solid State NMR and ^{127}I NQR. *Phys. Chem. Chem. Phys.* **2018**, *20* (30), 20043−20055.
(36) Barabash, A.; Gavrilko, T.; Eshimov, K.; Baran, J.; Ratajczak, H. ^{127}I NQR and Spectroscopic Investigation of Impurity-Doped and Mixed Lithium Iodate $Li_{1-x}H_xIO_3$ Crystals. *J. Mol. Struct.* **2004**, *708* (1−3), 113−116.
(37) Szell, P. M. J.; Grébert, L.; Bryce, D. L. Rapid Identification of Halogen Bonds in Co-Crystalline Powders via ^{127}I Nuclear Quadrupole Resonance Spectroscopy. *Angew. Chemie Int. Ed.* **2019**, *58* (38), 13479−13485.
(38) Bain, A. D.; Khasawneh, M. From NQR to NMR: The Complete Range of Quadrupole Interactions. *Concepts Magn. Reson. Part A An Educ. J.* **2004**, *22* (2), 69−78.
(39) Szell, P. M. J.; Bryce, D. L. Solid-state Nuclear Magnetic Resonance and Nuclear Quadrupole Resonance as Complementary Tools to Study Quadrupolar Nuclei in Solids. *Concepts Magn. Reson. Part A* **2016**, *45* (6), No. e21412.
(40) Sinyavsky, N.; Mershiev, I. Measuring of Short Spin-Spin Relaxation Times Distributions Using NQR Nutation Experiments. *Solid State Nucl. Magn. Reson.* **2019**, *104*, 101622.
(41) Massiot, D.; Farnan, I.; Gautier, N.; Trumeau, D.; Trokiner, A.; Coutures, J. P. ^{71}Ga and ^{69}Ga Nuclear Magnetic Resonance Study of β-Ga_2O_3: Resolution of Four-and Six-Fold Coordinated Ga Sites in Static Conditions. *Solid State Nucl. Magn. Reson.* **1995**, *4* (4), 241−248.
(42) Yamada, K.; Yamaguchi, T.; Ohashi, R.; Ohki, S.; Deguchi, K.; Hashi, K.; Goto, A.; Shimizu, T. Field-Stepwise-Swept QCPMG Solid-State ^{115}In NMR of Indium Oxide. *Solid State Nucl. Magn. Reson.* **2020**, *109*, 101688.
(43) Hung, I.; Altenhof, A. R.; Schurko, R. W.; Bryce, D. L.; Han, O. H.; Gan, Z. Field-stepped Ultra-wideline NMR at up to 36 T: On the Inequivalence between Field and Frequency Stepping. *Magn. Reson. Chem.* **2021**, *59* (9−10), 951−960.
(44) Xu, Y.; Calabrese, M.; Demitri, N.; Pizzi, A.; Nag, T.; Hung, I.; Gan, Z.; Resnati, G.; Bryce, D. L. Non-Covalent Matere Bonds in Perrhenates Probed via Ultrahigh Field Rhenium-185/187 NMR and

https://doi.org/10.1021/jacs.4c17499
J. Am. Chem. Soc. 2025, 147, 10823−10828

Zero-Field NQR Spectroscopy. *Chem. Commun.* **2023**, *59* (84), 12609−12612.
(45) Feyand, M.; Köppen, M.; Friedrichs, G.; Stock, N. Bismuth Tri- and Tetraarylcarboxylates: Crystal Structures, In Situ X-ray Diffraction, Intermediates and Luminescence. *Chem.—Eur. J.* **2013**, *19* (37), 12537−12546.
(46) Sudan, S.; Gładysiak, A.; Valizadeh, B.; Lee, J.-H.; Stylianou, K. C. Sustainable Capture of Aromatic Volatile Organic Compounds by a Pyrene-Based Metal−Organic Framework under Humid Conditions. *Inorg. Chem.* **2020**, *59* (13), 9029−9036.
(47) Babaryk, A. A.; Contreras Almengor, O. R.; Cabrero-Antonino, M.; Navalon, S.; Garcia, H.; Horcajada, P. A Semiconducting $Bi_2O_2(C_4O_4)$ Coordination Polymer Showing a Photoelectric Response. *Inorg. Chem.* **2020**, *59* (6), 3406−3416.
(48) Bryce, D. L.; Wasylishen, R. E. *Quadrupolar Nuclei in Solids: Influence of Different Interactions on Spectra*; John Wiley & Sons Ltd.: Chichester, 2012.
(49) Yamada, K.; Kaiho, T. Field-Stepwise-Swept Solid-State ^{127}I NMR of 1, 4-Diiodobenzene. *Solid State Nucl. Magn. Reson.* **2023**, *128*, 101905.
(50) Spiess, H. W.; Sheline, R. K. Quadrupole Coupling and Anisotropic Chemical Shifts in Some Manganese Carbonyls. *J. Chem. Phys.* **1971**, *54* (3), 1099−1103.
(51) Tran, D. T.; Chu, D.; Oliver, A. G.; Oliver, S. R. J. A 3-D Bismuth−Organic Framework Containing 1-D Cationic Inorganic $[Bi_2O_2]_2^+$ Chains. *Inorg. Chem. Commun.* **2009**, *12* (10), 1081−1084.
(52) Näther, C.; Jeß, I. Crystal Structure of $^{2}_{\infty}[Cu_2I_2$ (μ-4−4'-Bipyridine)] and Investigations on the Thermal Decomposition of CuX-4,4′-Bipyridine Coordination Polymers. *Monatshefte für Chemie/Chemical Mon* **2001**, *132* (8), 897−910.
(53) Zhang, W.; Lucier, B. E. G.; Terskikh, V. V.; Chen, S.; Huang, Y. Understanding Cu(I) Local Environments in MOFs via $^{63/65}$Cu NMR Spectroscopy. *Chem. Sci.* **2024**, *15* (18), 6690−6706.
(54) Bu, D.; Bu, D.; Chen, W.; Huang, C.; Li, L.; Lei, H.; Huang, S. Metal−Organic Frameworks with Mixed-Anion Secondary Building Units as Efficient Photocatalysts for Hydrogen Generation. *J. Catal.* **2022**, *407*, 10−18.
(55) Kemp, T. F.; Smith, M. E. QuadFit—A New Cross-Platform Computer Program for Simulation of NMR Line Shapes from Solids with Distributions of Interaction Parameters. *Solid State Nucl. Magn. Reson.* **2009**, *35* (4), 243−252.
(56) Bürgi, H. B. Motion and Disorder in Crystal Structure Analysis: Measuring and Distinguishing Them. *Annu. Rev. Phys. Chem.* **2000**, *51* (1), 275−296.
(57) Braga, D.; Maini, L.; Mazzeo, P. P.; Ventura, B. Reversible Interconversion between Luminescent Isomeric Metal−Organic Frameworks of $[Cu_4I_4(DABCO)_2]$(DABCO= 1,4-Diazabicyclo[2.2.2]Octane). *Chem.—Eur. J.* **2010**, *16* (5), 1553−1559.

https://doi.org/10.1021/jacs.4c17499
J. Am. Chem. Soc. 2025, 147, 10823−10828